Current distribution inside Py/Cu lateral spin-valve device

J. Hamrle,[1,2] T. Kimura,[1,2] Y. Otani,[1,2,3] K. Tsukagoshi,[4] and Y. Aoyagi[4]

[1] *FRS, The Institute of Physical and Chemical Research (RIKEN), 2-1 Hirosawa, Wako, Saitama 351-0198, Japan*
[2] *CREST, Japan Science & Technology Corporation, Japan*
[3] *ISSP, University of Tokyo, Kashiwa-shi, Chiba 277-8581, Japan*
[4] *RIKEN, 2-1 Hirosawa, Wako, Saitama 351-0198, Japan*

(Dated: February 2, 2008)

We have investigated experimentally the non-local voltage signal (NLVS) in the lateral permalloy (Py)/Cu/Py spin valve devices with different width of Cu stripes. We found that NLVS strongly depends on the distribution of the spin-polarized current inside Cu strip in the vicinity of the Py-detector. To explain these data we have developed a diffusion model describing spatial (3D) distribution of the spin-polarized current in the device. The results of our calculations show that NLVS is decreased by factor of 10 due to spin flip-scattering occurring at Py/Cu interface. The interface resistivity on Py/Cu interface is also present, but its contribution to reduction of NLVS is minor. We also found that most of the spin-polarized current is injected within the region 30 nm from Py-injector/Cu interface. In the area at Py-detector/Cu interface, the spin-polarized current is found to flow mainly close on the injector side, with $1/e$ exponential decay in the magnitude within the distance 80 nm.

PACS Numbers: 75.70.Pa, 75.70.Kw, 85.70.Kh

I. INTRODUCTION

Spintronics is a quickly evolving field providing the possibility to manipulate spin degrees of freedom in the solid state systems[1,2] . Spin injection, transport and detection in metals and semiconductors are of particular importance to construct effective spintronic devices such as a spin battery[3] and spin torque transistor[4] etc. Such devices have great advantages over the conventional electronic devices because of additional spin functionalities. To realize the device it is a key to obtain both large spin-polarized current and spin accumulation. It is also important to understand the diffusive nature of the spin-polarized currents in multiterminal devices.

Recently, the non-local probing method was proposed by Jedema *et al.*[5–7] to extract only spin-polarized current contribution from the spin-dependent phenomena and to reduce spurious effects such as Hall effect and anisotropic magnetoresistance. They succeeded in detecting the clear spin-accumulation signal in the vicinity of the non(N)-/ferro(F)-magnetic planar junction by the non-local spin-voltage (NLVS) even at room temperature[6,7]. Furthermore, non-local technique maybe useful to induce spin-injection magnetization reversal[8] without the charge current, leading to the solution for the energy dissipation problem due to Joule heat.

Here, we study experimentally the distribution of the spin-polarized current in non-local configuration. So far, the spin-polarized current transport is analytically investigated using one dimensional (1D) Boltzmann diffusion model[6,9–12]. As these models predict too large NLVS, we have developed formalism to calculate spatial (3D) distribution of spin-polarized current. However, large decrease of NLVS can not be attributed to spatial distribution of spin-polarized current, and we attribute it to spin scattering at Py/Cu interface.

II. DEVICE PREPARATION AND EXPERIMENTAL RESULTS

We fabricated lateral spin-valve devices consisting of two Py wires bridged by Cu strip by means of nanofabrication techniques. Figure 1 shows a scanning-electron-microscope (SEM) image for one of the fabricated devices. First, we fabricated both Py wires of width $w_{\mathrm{Py}} = 120\,\mathrm{nm}$ and of thickness $t_{\mathrm{Py}} = 20\,\mathrm{nm}$ with the spacing of $l_{\mathrm{Cu}} = 170\,\mathrm{nm}$ by electron-beam lithography and lift-off technique. Py layer was evaporated by an electron-beam gun at 2×10^{-8} Torr. Ends of the first Py wire are connected to large pads pattern for assisting the nucleation of the domain wall, although ends of the second one are flat-end shaped. Hence, each Py wire has different switching field.

Both Py wires are bridged by Cu strip of thickness

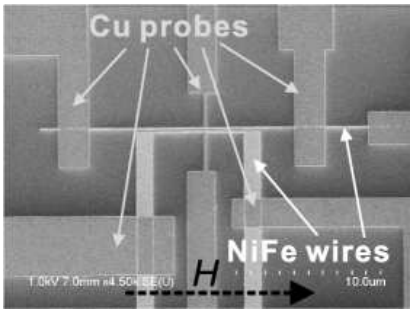

FIG. 1: SEM image of the fabricated lateral spin-valve device.

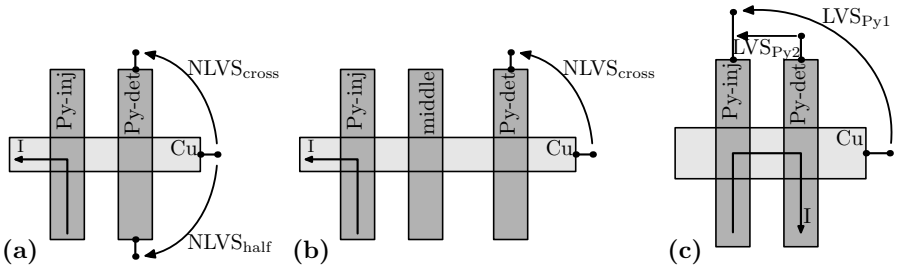

FIG. 2: DNLVS for system with (a) 2-wires and (b) with 3-wires. (c) Difference of *local* voltage signal (DLVS) for system with 2 wires.

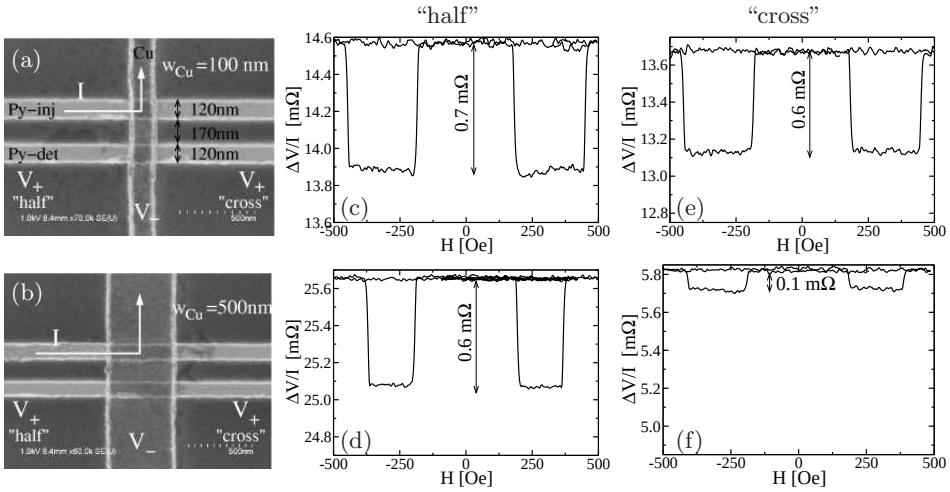

FIG. 3: (a)(b) SEM image of a detail of the lateral spin-valve device with $w_{\rm Cu}$ = 100, 500 nm, respectively, with sketched current flows and "cross" and "half" detection configuration. (c-f) NLVS as a function of external magnetic field, obtained for "cross" and "half" configuration for $w_{\rm Cu} = 100,\ 500$ nm.

$t_{\rm Cu} = 80$ nm, having widths $w_{\rm Cu}$ =100, 300 and 500 nm for three different devices. Prior to Cu deposition, the Py surface was cleaned by Ar^+ bombardment and then sample was shortly taken out-of-vacuum to change vacuum chamber. Then Cu was evaporated by resistance heating. The contact resistance of the interface was found ohmic and very low indicating a transparent contact. The conductivity of Cu is $\sigma_{\rm Cu,RT} = 48.1 \times 10^6\,\Omega^{-1}{\rm m}^{-1}$, $\sigma_{\rm Cu,4K} = 131 \times 10^6\,\Omega^{-1}{\rm m}^{-1}$ at room temperature, 4 K, respectively.

Notice that the present Cu strip has smaller residual resistivity than that of Jedema *at el.*[6]. The NLVS measurements were performed at room temperature with the magnetic field applied parallel along the Py-wires.

NLVS measurements were performed using a standard current-bias lock-in technique at room temperature. We measured the NLVS as a function of external magnetic field by using two different probe configurations, called "half" and "cross". The difference between both configurations is whether the current and voltage probes are located on the same side or not as sketched in Figs. 2(a) or 3(a). The one-dimensional (1D) diffusion model[12,13] predicts that the obtained NLVS should be the same. However, as the spin-polarized current has the spatial distribution, the NLVS shows the difference between both probe configurations.

Figures 3(c) and 3(e) show a NLVS for $w_{\rm Cu} = 100$ nm with "half" and "cross" probe configuration, respectively. The obtained difference of NLVS between parallel and antiparallel magnetization (DNLVS) is 0.7 mΩ and 0.6 mΩ at room temperature, respectively. Figures 3(d) and 3(f) show NLVS for $w_{\rm Cu} = 500$ nm with "half" and "cross" configurations, providing 0.6 and 0.1 mΩ, respectively.

Experimental values of DNLVS as a function of $w_{\rm Cu}$ are presented on Fig. 4(a). Experimental data show that the difference between "cross' and "half" in DNLVS increases with increasing $w_{\rm Cu}$.

The other parameters (at room temperature) used in our calculations are as follow: Py conductivity $\sigma_{\rm Py} = 7.3 \times 10^6\,\Omega^{-1}{\rm m}^{-1}$, Py bulk spin asymmetry coefficient $\beta = 0.7$ ($\sigma_{\uparrow,{\rm Py}} = \sigma_{\rm Py}(1+\beta)/2$, $\sigma_{\downarrow,{\rm Py}} = \sigma_{\rm Py}(1-\beta)/2$) (Refs.[14–16]), spin-flip lengths $\lambda_{\rm Py} = 4.3$ nm (Ref.[14]) and $\lambda_{\rm Cu} = 350$ nm (Ref.[13]). Py wires have width $w_{\rm Py} = 120$ nm, thickness $t_{\rm Py} = 20$ nm and separated by distance $l_{\rm Cu} = 170$ nm. The Cu strip has thickness $t_{\rm Cu} = 80$ nm with widths $w_{\rm Cu} = 100,\ 300,\ 500$ nm.

III. 1D CALCULATIONS OF DNLVS

In the literature, there are two models describing NLVS (and DNLVS) inside metallic lateral spin-valve device: one given by Jedema *et. al.*[13] and the other by Takahashi and Maekawa[12]. Both models approximate the device into 1D wire circuit, in which the propagation of electrochemical potential $\mu_{\uparrow/\downarrow}$ and spin-polarized current $J_{\uparrow/\downarrow}$ is described by standard Valet-Fert model[10]. At an intersection point of several wires (hereafter called node), e.g. intersection of Cu and Py wires, the boundary con-

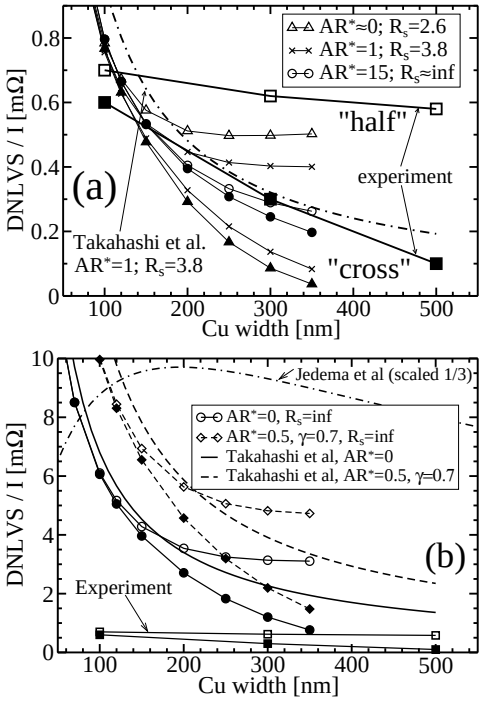

FIG. 4: Experimental value of DNLVS as a function of Cu wire width $w_{\rm Cu}$ compared with 1D and 3D models. Experimental data (square) compared with 1D and 3D models. $R^\star$ and R_s are interface and surface scattering resistances for Py/Cu interface, units in fΩm^2. For detail see Sec. III and IV B.

ditions, expressed as generalized Kirchoff's laws are

$$\begin{aligned} \sum_n J_{n,\uparrow/\downarrow} &= 0 \\ \mu_{n,\uparrow/\downarrow} &= \text{const}_{\uparrow/\downarrow} \end{aligned} \tag{1}$$

where n is an index of all the wires connected to a given node. Hence, the $\mu_{\uparrow/\downarrow}$ (which can be understand as a voltage here) is the same for each 1D wire attached to a given node, and $J_{\uparrow/\downarrow}$ is conserved while flowing through each node.

The model of Jedema *et al.*[13] has two assumptions, which are not fulfilled in our case of Py/Cu device: (a) they assume cross-sectional areas of all the wires in the device were the same (i.e. they considered more continuity of up and down current densities $j_{\uparrow/\downarrow}$ than up and down currents $J_{\uparrow/\downarrow}$ at each node) and (b) they assume $(\lambda_F, \lambda_N) \gg (w_F, w_N)$, where (w_F, w_N) are widths of F, N wires, respectively. The comparison of DNLVS obtained from this model (when extended to the case for different cross-sectional areas of wires) with our experimental data is shown on Fig. 4(b) (dashed-dot line), showing that this model predicts about 40× large value than experimental one.

These drawbacks were partly overcome by Takahashi and Maekawa[12], assuming that (a) $\lambda_F \ll (w_F, w_N) \ll \lambda_N$ and (b) that current at F/N interface is homogeneous. Later we will show that assumption (b) is not correct for ohmic junctions, but is correct for tunnel junctions. Although they derived their model from basic equations, the same results can be obtained when both F-injector and F-detector, attached to N wire, are described by a standard 1D model, where F-wires have effective cross-section area as of Py/Cu interface, i.e. in our case $\tilde{S}_F = w_F w_N$. The DNLVS calculated from this model is presented on Fig. 4(b) for the case with interface resistance $R^\star_{\rm Py/Cu} = 0$ (solid line) and $R^\star_{\rm Py/Cu} = 0.5\,f\Omega$m^2, $\gamma = 0.7$ (Ref.[15]) (dashed line). Note that $R^\uparrow_{\rm Py/Cu} = 2AR^\star_{\rm Py/Cu}(1-\gamma)$, $R^\downarrow_{\rm Py/Cu} = 2AR^\star_{\rm Py/Cu}(1+\gamma)$. This 1D model describes quite well the experimentally observed DNLVS but gives about 10 times larger magnitude than the experimental results.

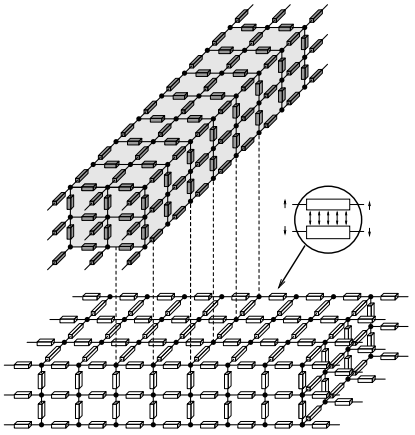

FIG. 5: The sketch of 3D network of spin-dependent-resistance-elements (SDRE). Circle inset sketches that SDRE consists of spin-up and spin-down resistances and of the shunting resistors between up and down channels. Note that each node and wire on the sketch represents a "bus" containing spin-up and spin-down channels.

IV. 3D CALCULATION OF SPIN-POLARIZED CURRENT AND ELECTROCHEMICAL POTENTIAL

In order to understand the spin-polarized currents inside device in detail, we have developed model calculating 3D distribution of $\mu_{\uparrow/\downarrow}$ and spin-polarized current density $j_{\uparrow/\downarrow}$ inside the device[17]. Our model is based on the 3D electrical network of spin-dependent-resistance-elements (SDRE) (Fig. 5). The response of each SDRE is determined by 1D models[10,13]. As sketched in inset of Fig. 5, each SDRE consists of resistance for spin-up, spin-down channels and spin-flip resistance shunting up and down channels. This shunting resistance can be regarded as the "probability" that electron spins are flipped when passing SDRE. A boundary conditions at each node connecting SDRE are given by Eq. (1).

In this model we can also account surface or interface resistance (scattering), $AR_{\rm ss}$ or AR_s, respectively, short-

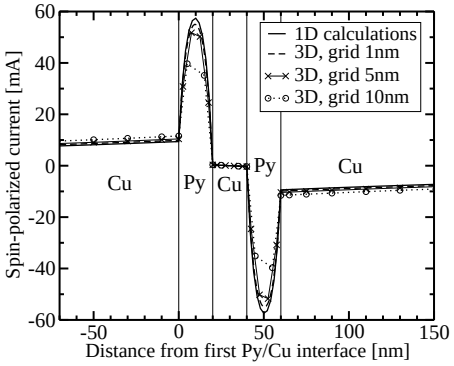

FIG. 6: The profile of $j_{\rm sp} = j_\uparrow - j_\downarrow$ through Cu/Py(20)/Cu(20)/Py(20)/Cu pillar structure, dimensions in nm, calculated for 1D VF model (full line) and compared with our 3D calculations with perpendicular-to-interface grid size 1 nm, 5 nm, 10 nm. Lateral (parallel-to-interface) grid size is 10 nm.

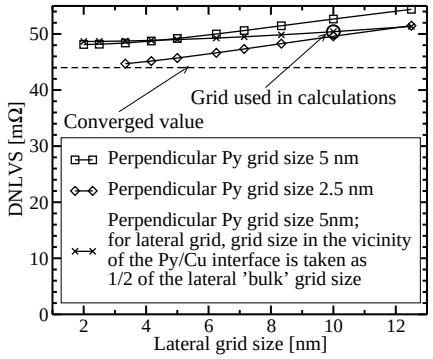

FIG. 7: Dependence of DNLVS on lateral grid size. Details in Sec. IV A.

cutting up and down channels at the surface or interface. For detailed description of the formalism please see[17].

A. Plausibility of 3D calculations

To estimate precision of our 3D calculations, we have calculated $j_{\uparrow/\downarrow}$, $\mu_{\uparrow/\downarrow}$ and magnetoresistivity ratio (MR) in Cu/Py(20)/Cu(20)/Py(20)/Cu *multilayer* structure (dimensions in nm) using different grid sizes for Py. The results of these calculations should be identical with 1D Valet-Fert model[10]. We investigate calculation precision only with grid size of Py, as $\lambda_{\rm Py} \ll \lambda_{\rm Cu}$.

Figure 6 shows profile of spin-polarized current $j_{\rm sp} = j_\uparrow - j_\downarrow$ through antiparallel Py/Cu multilayer structure. Used lateral grid size (i.e. grid distances parallel with Py/Cu interfaces) is 10 nm, perpendicular grid (i.e. grid perpendicular to interfaces) is 1, 5, 10 nm, giving $j_{\rm sp}$ precision inside Py being 4%, 9%, 15%, respectively. 3D calculations gives larger value of MR by 8%, 16%, 33% than 1D calculation. For in-plane grid size 5 nm, the MR is larger by 4%, 11%, 26%. It shows that (i) with decrease of grid size, $j_{\rm sp}$ and MR converge to correct values and (ii) small perpendicular grid size is more important than in-plane one.

Figure 7 shows a dependence of DNLVS in the lateral spin-valve structure on various lateral (i.e. parallel with substrate surface) grid size. The simulated device is different than real one; two Py wires of 15 nm-thick and 50 nm-width are separated by a distance of 80 nm and bridged by 55 nm-thick, 50 nm-width Cu strip.

DNLVS has been calculated for perpendicular grid size 5 nm (square in Fig. 7) and 2.5 nm (diamond), providing larger DNLVS by 18%, 11%, respectively, with respect to the converged DNLVS value. In both cases, larger grid size leads to larger DNLVS.

In all simulations of real structure, we used perpendicular grid size 5 nm, lateral grid size 10 nm and in the vicinity of Py/Cu interface lateral grid size 5 nm. This grid configuration is denoted by a circle on the Fig. 7, providing agreement with DNLVS converged value 13%, in agreement with above discussion. Unfortunately, in our calculations, we can not use smaller grid size due to numerical limitations. We conclude (i) precision of our 3D calculations is about 20% (ii) calculated DNLVS has tendancy to be overestimated.

B. 3D calculations of DNLVS

Figure 4(b) presents DNLVS calculated from 3D model for $AR^\star_{\rm Py/Cu} = 0$ (circle) and for $AR^\star_{\rm Py/Cu} = 0.5\,{\rm f}\Omega{\rm m}^2$, $\gamma = 0.7$ (Ref.[15]) (diamond). Both DNLVS have about the same shape and slightly smaller magnitude compared to values from 1D model by Takahashi and Maekawa[12] (solid and dashed lines without symbols). In agreement with experiment, for larger $w_{\rm Cu}$, the DNLVS has different values in half and cross configuration, reflecting inhomogeneous $j_{\rm sp}$ at position of the detector. As will be shown in Sec. V, the $j_{\rm sp}$ is also strongly inhomogeneous at injector position. However, the approximative agreement between 3D models and 1D models shows, that influence of inhomogeneous current injection is not very important to magnitude of DNLVS. As our 3D models tends to overestimate DNLVS, we conclude that non-local current injection decrease DNLVS, but only about 20%.

Both 1D and 3D models shows that the presence of $R^\star_{\rm Py/Cu}$ together with large positive value of γ increases DNLVS. When $R^\star_{\rm Py/Cu} > 0$, $\gamma = 0$, DNLVS decreases. It may be possible that $\gamma > 0$, but this contribution to DNLVS is smeared by other contribution decreasing DNLVS. Therefore, in following we assume $\gamma = 0$.

Now, let us discuss which mechanism decrease DNLVS. To be more sure with analysis, we take into account more experimental data (which are going to be published elsewhere[18]) on two different samples, fabricated exactly by a way as previous sample.

- 3-wires system consisting of two Py wires of 20 nm-thick, 100 nm-width, separated by a distance of 400 nm and bridged by 80 nm-thick 100 nm-width Cu strip. Between both Py wires, there is third 100 nm-width wire [Fig. 2(b)], consisting either of Cu (having thickness 80 nm), or Py wire (having thickness 20 nm), or there

	experiment	$AR^{\star}_{\mathrm{Py/Cu}}=0$, $AR_{s,\mathrm{Py/Cu}}=\inf$	$AR_{\mathrm{ss,Cu}}=0.15$	$AR_{\mathrm{ss,Cu,side}}=0.065$	$AR^{\star}_{\mathrm{Py/Cu}}\approx 0$, $AR_{s,\mathrm{Py/Cu}}=2.6$	$AR^{\star}_{\mathrm{Py/Cu}}=0.3$, $AR_{s,\mathrm{Py/Cu}}=3.1$	$AR^{\star}_{\mathrm{Py/Cu}}=1$, $AR_{s,\mathrm{Py/Cu}}=3.8$	$AR^{\star}_{\mathrm{Py/Cu}}=3$, $AR_{s,\mathrm{Py/Cu}}=8.2$	$AR^{\star}_{\mathrm{Py/Cu}}=15$, $AR_{s,\mathrm{Py/Cu}}\approx\inf$
$\mathrm{DNLVS_{half}}$, $w_{\mathrm{Cu}}=100$	0.7	6.1	0.77	0.74	0.78	0.81	0.76	0.87	0.79
$\mathrm{DNLVS_{cross}}$, $w_{\mathrm{Cu}}=100$	0.62	6.06	0.75	0.73	0.76	0.79	0.75	0.87	0.79
$\mathrm{DNLVS_{half}}$, $w_{\mathrm{Cu}}=300$	0.6	3.1	0.66	0.87	0.49	0.47	0.40	0.40	0.29
$\mathrm{DNLVS_{cross}}$, $w_{\mathrm{Cu}}=300$	0.3	1.2	0.07	0.24	0.08	0.11	0.14	0.21	0.25
3-wires, no middle	0.25	3.72	0.034	0.032	0.45	0.47	0.46	0.54	0.48
3-wires, Cu middle	0.18	2.53	0.025	0.033	0.32	0.33	0.31	0.35	0.28
3-wires, Py middle	0.04	0.76	0.019	0.018	0.037	0.052	0.075	0.16	0.33
$\mathrm{DNLVS_{half}}$, $w_{\mathrm{Cu}}=250$	×	0.51	2.0	0.61	0.29	0.29	0.25	0.27	0.25
$\mathrm{DNLVS_{cross}}$, $w_{\mathrm{Cu}}=250$	0.4	1.3	0.20	0.33	0.12	0.14	0.15	0.21	0.24
$\mathrm{DLVS_{2Py}}$, $w_{\mathrm{Cu}}=250$	1	3.8	2.0	2.2	0.50	0.50	0.46	0.51	0.50
$\mathrm{DLVS_{1Py}}$, $w_{\mathrm{Cu}}=250$	0.4	2.4	1.7	1.8	0.34	0.32	0.28	0.29	0.26

TABLE I: Experimental values of DNLVS (in mΩ) for various sample structures compared with values calculated by 3D models taking into account different processes decreasing DNLVS. Units of resistances are in fΩm^2, units of wire widths in nm. For details see Sec. IV B.

is no third-wire.

- system consisting of two Py 20 nm-thick wires with different widths (200 nm-width of injector and 100 nm-width of detector), separated by 200 nm and bridged by 250 nm-width and 80 nm-thick Cu strip. In this device, we measured both DNLVS and difference of *local* voltage signal between parallel and antiparallel state (DLVS) [Fig. 2(c)]. In DLVS case, charge current flows through both Py wires.

In the following, we will discuss possible contributions coming from (i) surface scattering on Cu, $AR_{\mathrm{ss,Cu}}$ (ii) surface scattering at Py/Cu interface $AR_{s,\mathrm{Py/Cu}}$ (iii) interface non-polarized resistance, $AR^{\star}_{\mathrm{Py/Cu}}$. The possible magnitude of each contribution has been determined to fit DNLVS for $w_{\mathrm{Cu}}=100$ nm and then compared with other experimental data. All experimental data and calculated values are summarized in Tab. I.

1. Surface scattering on Cu

Surface scattering on Cu is introduced by an resistance $AR_{\mathrm{ss,Cu}}$ shortcutting up and down channel on the Cu surface. To decrease DNLVS for $w_{\mathrm{Cu}}=100$ nm to experimental value, 0.7 mΩ, Cu surface scattering has to be $R_{\mathrm{ss,Cu}}=0.15$ fΩm^2 (when surface scattering is assumed on both side sides and top and bottom surface of Cu wire) or $R_{\mathrm{ss,Cu,side}}=0.065$ fΩm^2 (when surface scattering is assumed to be only on both sides of Cu). However, using those surface scattering resistances, the DNLVS calculated for 3-wires system (Tab. I) are too small compared with experiment, showing that this contribution is not a dominant one.

2. Interface scattering on Py/Cu interface

The properties of Py/Cu interface is here described by a presence of the interface layer, which has its own thickness t_I, spin-flip-length λ_I and conductivity σ_I, spin-polarization γ_I[19]. However, the interface properties should not depend on t_I (this value is given *ad-hoc* and is assumed as 1 nm in our calculations). Therefore, it is profitable to express interface properties by $\delta_I=t_I/\lambda_I$ and $AR^{\star}_{\mathrm{Py/Cu}}=t_I/\sigma_I$, which are independent on t_I[19]. Physical meaning of $AR^{\star}$ is clear: $2R^{\star}(1-\gamma_I)$, $2R^{\star}(1+\gamma_I)$ is a resistance of channel up, down through interface layer, respectively. As physical meaning of δ_I is not so clear, we prefer to describe spin-flip scattering by interface scattering resistivity[17]

$$AR_s=AR^{\star}\frac{4}{\delta\sinh\delta}, \tag{2}$$

which means a resistance shortcutting up and down channels on the interface.

To decrease DNLVS to experimental value at $w_{\mathrm{Cu}}=100$ nm, different pairs of $AR^{\star}_{\mathrm{Py/Cu}}$, $AR_{s,\mathrm{Py/Cu}}$ can be used, as shown in Table I. When there is no interface resistance ($AR^{\star}_{\mathrm{Py/Cu}}=0$), then $AR_{s,\mathrm{Py/Cu}}=2.6$ fΩm^2. On the other

hand, when $AR_{s,\mathrm{Py/Cu}} = \mathrm{inf}$ then $AR^{\star}_{\mathrm{Py/Cu}} = 15\,\mathrm{f\Omega m^2}$. Both $AR_{s,\mathrm{Py/Cu}}$ and $AR^{\star}_{\mathrm{Py/Cu}}$ contribute to decrease of DNLVS.

Table I and Figure 4(a) shows that none combination of pairs $AR^{\star}_{\mathrm{Py/Cu}}$, $R_{s,\mathrm{Py/Cu}}$ describes perfectly all experimental values, however the agreement with all experimental data is within factor of 2-3. Figure 4(a) shows that with increasing value of $AR^{\star}_{\mathrm{Py/Cu}}$, the difference between "half" and "cross" DNLVS is reducing, reflecting more homogeneous injection of j_{sp} over Py-inj/Cu interface.

The most relevant interface properties is a pair of values $AR^{\star}_{\mathrm{Py/Cu}} = 1\,\mathrm{f\Omega m^2}$, $R_{s,\mathrm{Py/Cu}} = 3.8\,\mathrm{f\Omega m^2}$ ($\delta_{\mathrm{Py/Cu}} = 0.95$) as for this pair the mutual ratio between DNLVS's for 3-wire system (when middle wire is Cu, Py and nothing) agrees with experiment. Then all calculated values for 3-wires systems are about 1.8× larger then experimental one. The disagreement by factor 1.8× can be related to smaller value of λ_{Cu} than expected 350 nm. The 3-wire configuration with middle Py wire is particularly sensitive to $AR^{\star}_{\mathrm{Py/Cu}}$, as its value determines, how large amount of j_{sp} is absorbed by the middle Py wire.

Table I shows that experimental value of DNLVS at $w_{\mathrm{Cu}} = 300\,\mathrm{nm}$ is larger than calculated one, particularly for cross configuration (experimental $\mathrm{DNLVS_{cross}} = 0.3\,\mathrm{m\Omega}$, but calculated $0.14\,\mathrm{m\Omega}$). In another words, $\mathrm{DNLVS}(w_{\mathrm{Cu}})$ decreases slower for experiment than for calculated value. It is probably due to presence of a charge current j_{ch} at a position of Py-detector for wider w_{Cu}, as will be shown in Sec. V B. Non-zero j_{ch} inside detector probably causes some additive contribution to DNLVS, either due to AMR, either due to the scattering related with currents in-plane (CIP), i.e. currents flowing parallel with Py/Cu interface

Figure 4(b) also contain a dependence $\mathrm{DNLVS}(w_{\mathrm{Cu}})$ calculated from extended model of Takahashi and Maekawa for $AR^{\star}_{\mathrm{Py/Cu}} = 1\,\mathrm{f\Omega m^2}$, $R_{s,\mathrm{Py/Cu}} = 3.8\,\mathrm{f\Omega m^2}$. We can see that there is a good agreement with 3D calculations. It shows when j_{sp} is homogeneous on detector position, this model predicts a correct value of DNLVS.

The last part of Table I shows an agreement between experimental and calculated values of DNLVS and DLVS, determined for $w_{\mathrm{Cu}} = 250\,\mathrm{nm}$. We can see that for $AR^{\star}_{\mathrm{Py/Cu}} = 1\,\mathrm{f\Omega m^2}$, $R_{s,\mathrm{Py/Cu}} = 3.8\,\mathrm{f\Omega m^2}$, all experimental values are about twice large compared to calculated one. Probably, here play role similar effects as discussed for DNLVS for $w_{\mathrm{Cu}} = 300\,\mathrm{nm}$, as in this case calculated DNLVS is also twice smaller than experimental one.

Resistance $AR^{\star}_{\mathrm{Py/Cu}} = 1\mathrm{f\Omega m^2}$ is equal to resistance of 48 nm of Cu or 7.3 nm of Py. Furthermore, interface scattering $AR_{s,\mathrm{Py/Cu}} = 3.8\mathrm{f\Omega m^2}$ corresponds to scattering by Cu at length 950 nm and at length 2.5 nm inside Py [Eq. (2)]. Especially second value shows that interface scattering is not so large, however, it is enough to decrease DNLVS by one order of magnitude.

In conclusion of this Section, we have shown that major contribution to small DNLVS is due to interface scattering resistance $AR_{s,\mathrm{Py/Cu}}$, shortcutting up and down channels at Py/Cu interfaces. The interface resistivity $AR^{\star}_{\mathrm{Py/Cu}}$ is also presented, but its contribution to decrease of DNLVS is only minor one. Such a large interface spin-scattering has not been observed in[14,15]. It can be related with two factors:

1. Quality of our Py/Cu interface is lower than in[14,15]. In our fabrication process, there are two steps which could decrease interface quality. On top of Py we deposited and removed photoresist to pattern Cu wire. Before Cu deposition, the surface was cleaned by Ar^{+} bombardment and then device shortly taken out of vacuum to change vacuum chamber. Notice, that Jedema et al.[13] has used very similar fabrication process as we did.

2. Contribution of Py/Cu interface spin scattering is missing in previous works, investigating Py/Cu system by means of magnetoresistivity ratio (MR)[14,15]. Note that MR is sensitive to value of j_{sp} passing free layer rather that to value of spin accumulation $\Delta\mu$ at position of free layer[17]. As we have shown[17], system can provide large MR (when large j_{sp} flow through free layer) although $\Delta\mu$ at position of free layer can vanish. When $\Delta\mu$ vanishes, then shortcutting of up and down channels takes no effect and so interface spin-scattering does not occurs at the interface. In such a case, the MR (up to some limit) is insensitive to spin-scattering on the free-layer/non-magnetic-layer interface.

   On the other hand, non-local technique is particularly sensitive to $\Delta\mu$ at detector/non-magnetic-metal interface. When interface spin-scattering is presented in this case, it significantly reduces DNLVS.

   Hence, it may be possible, that small interface scattering is presented in both MR and non-local measurements, but did not take a place in case of MR measurements.

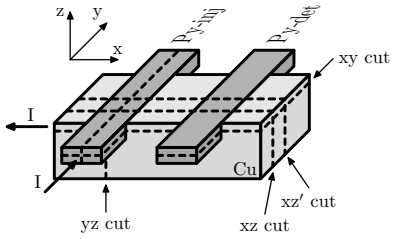

FIG. 8: The sketch of the device with indicated cut planes. The yz, xz′ cuts are taken in the center of Py-injector, Cu wire, respectively. The xy cut is located 12.5 nm from device top, the xz cut is located 7.5 nm from the side of Cu wire.

V. CURRENT FLOWS INSIDE LATERAL SPIN-VALVE STRUCTURE

In this Section, we present in detail the current inhomogeneity inside lateral spin-valve structure. Figure 8 shows a sketch of the device with indicated cut planes, on which the calculated current densities are presented on Figures 9, 11, 12, 13 and discussed in following Sections V A–V C. The presented current densities were calculated for parallel magnetizations and for our best interface description $AR^{\star}_{\mathrm{Py/Cu}} = 1\,\mathrm{f\Omega m^2}$, $R_{s,\mathrm{Py/Cu}} = 3.8\,\mathrm{f\Omega m^2}$. For antiparallel magnetizations, we get very similar current flows as for parallel one. This is in agreement with 1D models of non-local devices[12,13], where current flows are exactly the same for parallel and antiparallel magnetic states.

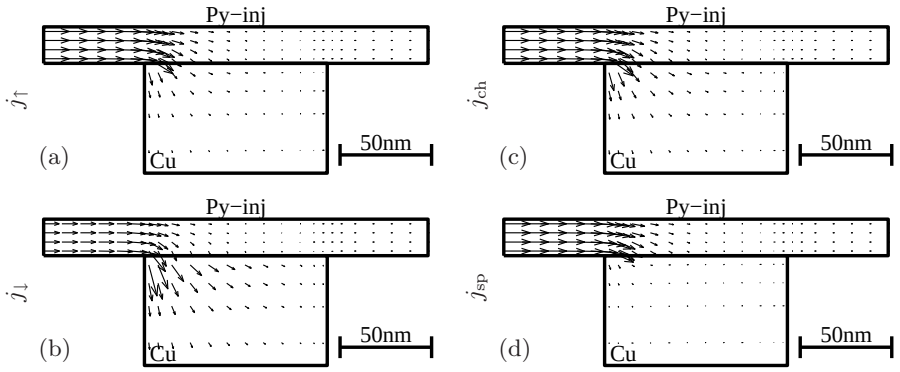

FIG. 9: The yz cut (defined on Fig. 8) of the current density of (a) current polarized up $j_\uparrow$ (b) current polarized down $j_\downarrow$ (c) charge current $j_{\rm ch} = j_\uparrow + j_\downarrow$ and (d) spin-polarized current $j_{\rm sp} = j_\uparrow - j_\downarrow$ in the device with $w_{\rm Cu} = 100\,{\rm nm}$ with parallel magnetization. The length of arrow is proportional to value of a given current; this scaling is the same for all cuts.

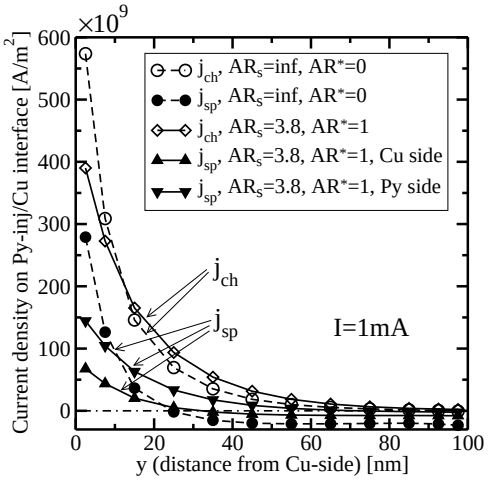

FIG. 10: The profiles of $j_{\rm ch}$ (open symbols) and $j_{\rm sp}$ (solid symbols) taken at the intersection of Py-injector/Cu interface and the yz cut (Fig. 8). The profiles were calculated for $w_{\rm Cu} = 100\,{\rm nm}$, for current I=1 mA, for $AR^\star_{\rm int} = 0$, $AR_{s,{\rm Py/Cu}} = {\rm inf}$ (circle) and for $R^\star_{\rm int} = 1{\rm f}\Omega{\rm m}^2$, $AR_{s,{\rm Py/Cu}} = 3.8\,{\rm f}\Omega{\rm m}^2$ (triangles and diamond). $j_{\rm sp}$ and $j_{\rm ch}$ are the same for parallel and anti-parallel magnetizations. The symbols denote grid, for which the current densities are calculated.

A. Current description near Py-injector

Figure 9 shows current density on the yz cut, which is taken in the center of the Py-injector wire (Fig. 8). Cuts (a–d) correspond to the cases for up and down current densities $j_\uparrow$, $j_\downarrow$, respectively, for charge current density $j_{\rm ch} = j_\uparrow + j_\downarrow$ and for spin-polarized current density $j_{\rm sp} = j_\uparrow - j_\downarrow$. All cuts show that the current is injected rather sharply through Py-injector/Cu interface and then quickly spreads into the whole volume of Cu wire.

The values of $j_{\rm ch}$ and $j_{\rm sp}$ at the intersection of yz cut and Py-injector/Cu interface are presented on Fig. 10. The profile is shown for the device with $AR^\star_{\rm Py/Cu} = 0$, $AR_{s,{\rm Py/Cu}} = {\rm inf}$ (circles) and for $AR^\star_{\rm Py/Cu} = 1\,{\rm f}\Omega{\rm m}^2$, $R_{s,{\rm Py/Cu}} = 3.8\,{\rm f}\Omega{\rm m}^2$ (triangles and diamond). Due to spin-flip-scattering on the interface, the $j_{\rm sp}$ flowing to the interface from Py side (triangles-down) is about twice larger than from $j_{\rm sp}$ outgoing the interface at Cu side (triangles-up).

It is shown that both $j_{\rm ch}$ (open symbols) and $j_{\rm sp}$ (solid symbols) are sharply injected within the distance of 25 nm, 35 nm from the Py/Cu edge for $AR^\star_{\rm Py/Cu} = 1\,{\rm f}\Omega{\rm m}^2$, $AR_{s,{\rm Py/Cu}} = 3.8\,{\rm f}\Omega{\rm m}^2$ and $AR^\star_{\rm Py/Cu} = 0$, $AR_{s,{\rm Py/Cu}} = {\rm inf}$ respectively. This different 'length-of-injection' is only due to different values of $AR^\star_{\rm Py/Cu}$, and is nearly independent on $AR_{s,{\rm Py/Cu}}$. When $R^\star_{\rm Py/Cu}$ is large then obviously the current is more spread over the interface and for tunnel contacts is can be considered as homogeneous. Furthermore, $j_{\rm sp}$ is positive only in the distance of 25 nm or 35 nm from the Py-injector/Cu edge, and then its value becomes negative. This means that in this region the injector reabsorbs a small part of the injected spin-polarized current, which decreases the spin-injection efficiency.

For different values of $w_{\rm Cu}$, the 'length-of-injections' are very similar to those presented in Fig. 10. It should be noticed that this sharp injection occurs in consequence of small Py conductivity, $\sigma_{\rm Py} \ll \sigma_{\rm Cu}$ and small thickness of Py wire $t_{\rm Py} < (w_{\rm Cu}, t_{\rm Cu})$. In other words, larger $t_{\rm Py}$ increases homogeneity of the injected current.

B. Top view on Cu

Figure 11 presents current density on xy cut (defined in Fig. 8) taken at the depth of 12.5 nm from top surface of the Cu wire. As already discussed, current is sharply injected at Cu/Py-injector edge and hence $j_\uparrow$ and $j_{\rm sp}$ spread into the Cu wire from this edge [Fig. 11(a)(d)].

Figure 11(d) also shows that for $w_{\rm Cu} = 100\,{\rm nm}$, $j_{\rm sp}$ at the position of the detector is fairly uniform in the y-direction, i.e. in the direction parallel to the Py wire. When $j_\uparrow$ reaches detector, it is successively spin-scattered due to very short spin-diffusion length $\lambda_{\rm Py}$ and then current flows homogeneously back as $j_\downarrow$ [Fig. 11(a)(b)].

Due to the sharp current injection, $j_{\rm ch}$ makes a whirl in the 'diffusive' part of the Cu wire, where no charge current was expected [Figure 11(c)]. In the present case ($w_{\rm Cu} = 100\,{\rm nm}$), the value of $j_{\rm ch}$ originating from this whirl at detector position is negligible compared to $j_{\rm sp}$. However when $l_{\rm Cu} < w_{\rm Cu}$ ($l_{\rm Cu}$ being distance between Py wires), then $j_{\rm ch} \gtrapprox j_{\rm sp}$ at detector position. This can be seen on Fig. 12(a) for $w_{\rm Cu} = 300\,{\rm nm}$. Fig. 12(b) shows that also $j_{\rm sp}$ for $w_{\rm Cu} = 300\,{\rm nm}$ is inhomogeneous at detector position, having maximal value at one side of Cu/Py-detector interface. This explains different values between "cross" and "half" configurations.

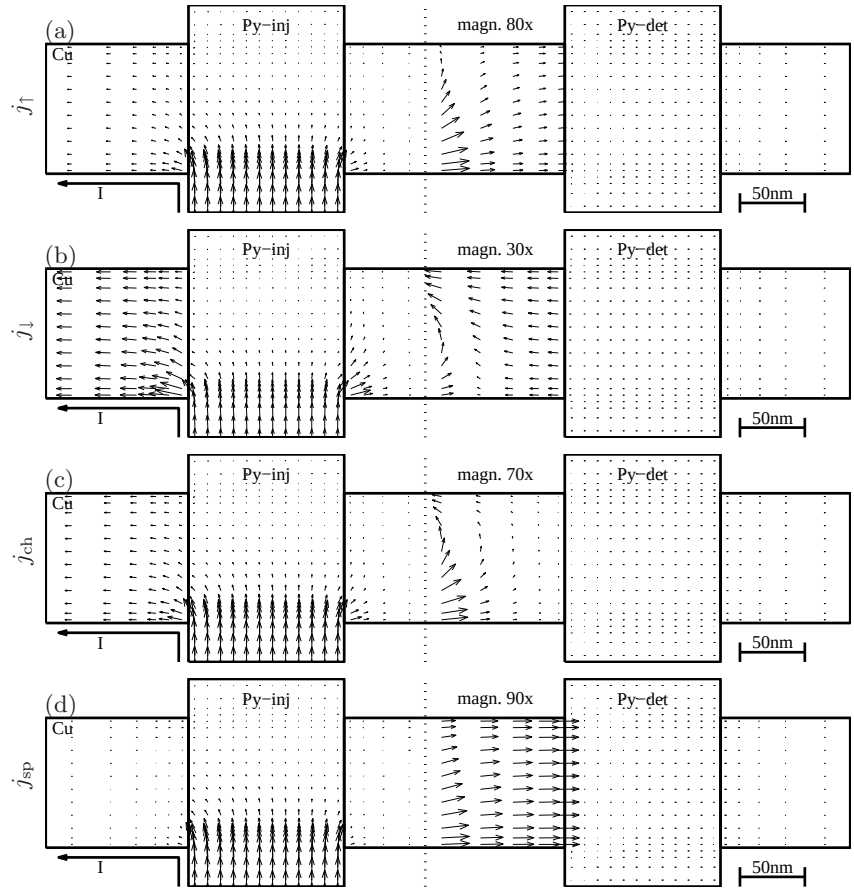

FIG. 11: The xy cut (defined on Fig. 8) of (a) $j_\uparrow$ (b) $j_\downarrow$ (c) $j_{\rm ch}$ and (d) $j_{\rm sp}$ in the device with $w_{\rm Cu} = 100\,{\rm nm}$, parallel magnetization. The arrows have the same scaling for all cuts, and they are magnified on cut's right sides.

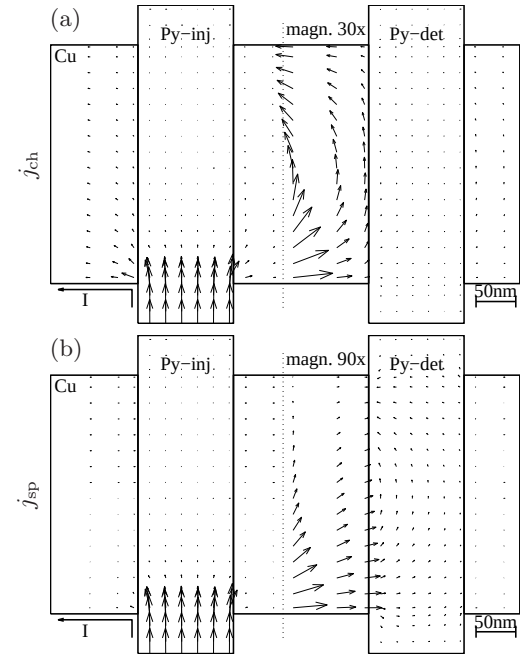

FIG. 12: The xy cut (defined on Fig. 8) of (a) $j_{\rm ch}$ and (b) $j_{\rm sp}$ in the device with $w_{\rm Cu} = 300\,{\rm nm}$. The arrows have the same scaling for all cuts, and they are magnified on cut's right sides.

C. Current description near Py-detector

Figure 13 presents current density on the xz cut (defined in Fig. 8) which is taken 7.5 nm from the side of Cu wire. Figure 13(a) shows that the flow of $j_\uparrow$ into detector is also inhomogeneous and is dominant at the side of Py-detector/Cu, which is close to the injector. As already mentioned above, due to very short spin-diffusion length $\lambda_{\rm Py} = 4.3\,{\rm nm}$, $j_\uparrow$ flowing into the detector is immediately reversed inside Py-detector and coming back as $j_\downarrow$ [Fig. 13(b)]. This can be understand as a resistance shunting (or "short-cutting") the up and down channels. This also explains the behaviour of $j_{\rm sp}$ [Fig. 13(d)], whose flow is absorbed by the detector.

Figure 14 shows $j_{\rm ch}$ and $j_{\rm sp}$ on the intersection between Py-detector/Cu interface and xz′ cut (defined on Fig. 8), which is taken at the center of Cu wire. The vertical dash-dot lines show the position of edges inside Py-detector wire embedded in the Cu wire, i.e. ranges $x \in (-20, 0)$ and $x \in (120, 140)$ corresponds to side part of Py wire, although range $x \in (0, 120)$ represents bottom part of Py-detector wire. We can see that both $j_{\rm sp}$ and $j_{\rm ch}$ are inhomogeneous, decaying approximately exponentially with $1/e$ decrease length 80 nm. This decay is mainly result of the competition between Cu conductivity $\sigma_{\rm Cu}$ and spin-flip scattering inside Py and Py/Cu interface.

When the interface resistances $AR^\star_{\rm Py/Cu} = 1\,{\rm f\Omega m^2}$, $AR_{s,{\rm Py/Cu}} = 3.8\,{\rm f\Omega m^2}$ are introduced, $j_{\rm sp}$ flowing to the detector is decreased (and hence DNLVS is decreased), as can be seen on Fig. 14. Due to presence of $AR_{s,{\rm Py/Cu}}$, the current flowing to the interface from Cu side (triangle-up) is about

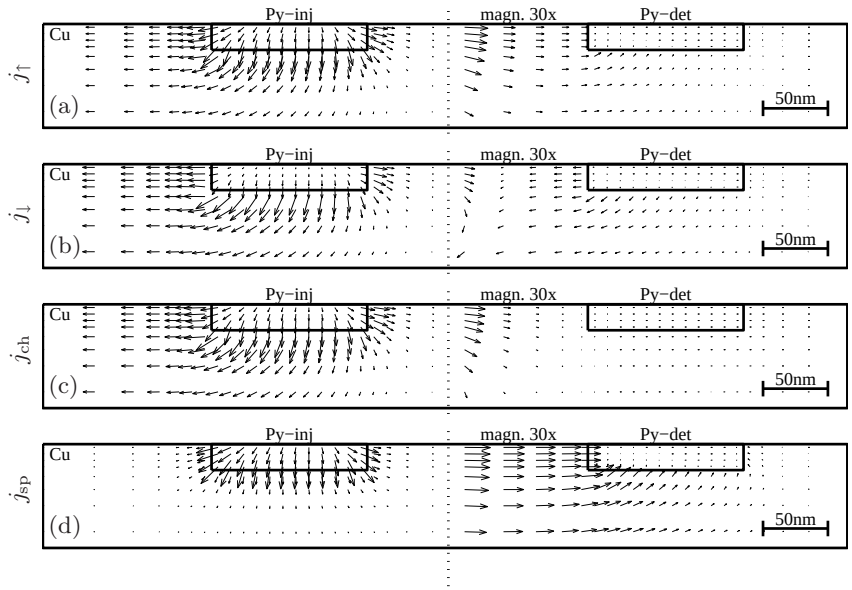

FIG. 13: The xz cut (defined on Fig. 8) of (a) $j_\uparrow$ (b) $j_\downarrow$ (c) $j_{\rm ch}$ and (d) $j_{\rm sp}$ in the device with $w_{\rm Cu} = 100\,{\rm nm}$, parallel magnetization. The arrows have the same scaling for all cuts, and they are magnified on cut's right sides.

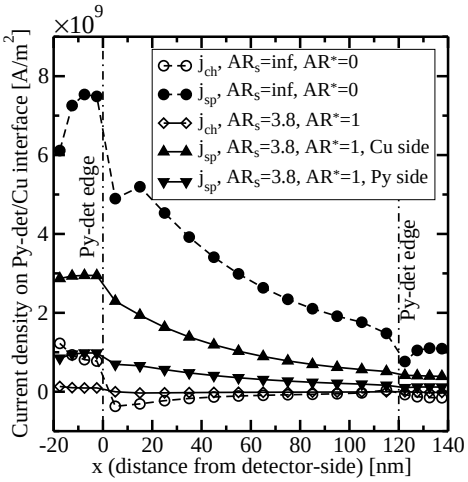

FIG. 14: The profile of $j_{\rm ch}$ and $j_{\rm sp}$ on the intersection of Py-detector/Cu interface and the xz' cut (defined on Fig. 8) for parallel magnetization state. The rest as in Fig. 10.

3× larger than one outgoing to the injector (triangle down). Hence, 2/3 of $j_{\rm sp}$ entering detector are shortcut, absorbed by a interface.

There is also $j_{\rm ch}$ at Py-detector/Cu interface, having value about 10% of $j_{\rm sp}$. The $j_{\rm ch}$ originates because $j_\uparrow$ and $j_\downarrow$ are injected to/ejected from the Py-detector at slightly different position, i.e. $j_{\rm ch}$ has negative value around $x \gtrsim 0$ and positive at $x \lesssim 0$. It means that part of $j_\uparrow$ current, which is injected to Py-detector from the side of the Py wire, is ejected as $j_\downarrow$ from its top part.

VI. CONCLUSION

We have fabricated lateral spin-valve devices consisting of the permalloy (Py) and Cu wires. We have observed that the difference of the non-local voltage signal (DNLVS) between parallel and antiparallel magnetization has different values for "half" and "cross" configurations. The difference between these two configurations increases when the width of the Cu stripe increases.

To understand observed behaviour in detail, we have developed formalism calculating spatial (3D) distribution of the spin-polarized current and electrochemical potential inside the device. We found that the current distribution inside lateral spin-valve device with ohmic-contact is rather complex interplay between geometry and electrical properties of all the involved materials.

Despite of those large current inhomogeneities, the DNLVS calculated from our 3D model are in a good agreement with 1D model given by Takahashi et Maekawa[12]. However, both 1D and 3D predicts about 10× larger DNLVS than experimental values. We have attributed the smallness of DNLVS to interface scattering resistance $AR_{s,{\rm Py/Cu}} = 3.8{\rm f}\Omega{\rm m}^2$ shortcutting up and down channels at Py/Cu interface. On one hand, this value of $AR_{s,{\rm Py/Cu}}$ decrease DNLVS by factor of 10. On the other hand, it corresponds only to scattering which occurs inside Py on distance of 2.5 nm. When this interface scattering resistance can be reduced, DNLVS may be enhanced significantly. The fact, that such a interface resistivity has not been observed before[14,15] may be related either to lower quality of our interface, either to insensitivity of MR to small surface scattering in some cases.

Interface resistance $AR^\star_{\rm Py/Cu} = 1{\rm f}\Omega{\rm m}^2$ is also presented at Py/Cu interface, but its contribution to smallness of DNLVS is minor. The value of this resistance mainly modifies the $j_{\rm sp}$ inhomogeneity in the structure. Using this description of Py/Cu interface, we found agreement with all our experimental data (local and non-local voltage signals measured on systems with two or three Py wires) within factor of two.

The current is injected from Py-injector to Cu sharply, within the distance of 30 nm. Part of the injected spin-polarized current is reabsorbed by injector itself. Current flow over Py-detector/Cu interface is also inhomogeneous, having the largest value on the side of Py-detector close to injector and decaying approximately exponentially with $1/e$ decrease within the distance 80 nm.

[1] M. Ziese and M. Thornton, editors, *Spin electronics* (Springer, Berlin, 2001).
[2] I. Zutic, J. Fabian, and S. Das Sarma, Rev. Mod. Phys. **76**, 1 (2004).
[3] A. Brataas, Y. Tserkovnyak, G. E. W. Bauer, and B. I. Halperin, Phys. Rev. B **66**, 060404R (2002).
[4] G. E. W. Bauer, Y. Tserkovnyak, D. Huertas-Hernando, and A. Brataas, Phys. Rev. B **67**, 094421 (2003).
[5] F. J. Jedema, B. J. van Wees, B. H. Hoving, A. T. Filip, and T. Klapwijk, Phys. Rev. B **60**, 16549 (1999).
[6] F. J. Jedema, A. T. Filip, and B. J. van Wees, Nature **410**, 345 (2001).
[7] F. J. Jedema, H. B. Heersche, A. T. Filip, J. J. A. Baselmans, and B. J. van Wees, Nature **416**, 713 (2002).
[8] J. A. Katine, F. J. Albert, R. A. Buhrman, E. B. Myers, and D. C. Ralph, Phys. Rev. Lett. **84**, 3149 (2000).
[9] P. C. van Son, H. van Kempen, and P. Wyder, Phys. Rev. Lett. **58**, 2271 (1987).
[10] T. Valet and A. Fert, Phys. Rev. B **48**, 7099 (1993).
[11] S. Takahashi and S. Maekawa, Phys. Rev. Lett. **88**, 116601 (2002).
[12] S. Takahashi and S. Maekawa, Phys. Rev. B **67**, 052409 (2003).
[13] F. J. Jedema, M. S. Nijboer, A. T. Filip, and B. J. van Wees, Phys. Rev. B **67**, 085319 (2003).
[14] S. Dubois *et al.*, Phys. Rev. B **60**, 477 (1999).
[15] S. Steenwyk, S. Hsu, R. Loloee, J. Bass, and W. Pratt, Jr., J. of Magn. Magn. Mater. **170**, L1 (1997).
[16] P. Holody *et al.*, Phys. Rev. B **58**, 12230 (1998).
[17] J. Hamrle, T. Kimura, T. Yang, and Y. Otani, cond-mat/0409309.
[18] T. Kimura, J. Hamrle, and Y. Otani, to be published.
[19] W. Park *et al.*, Phys. Rev. B **62**, 1178 (2000).